

Comparison of ^3He and ^{129}Xe MRI for Evaluation of Lung Microstructure and Ventilation at 1.5T

Neil J. Stewart, PhD,¹ Ho-Fung Chan, MEng,¹ Paul J.C. Hughes, MEng,¹
 Felix C. Horn, PhD,¹ Graham Norquay, PhD,¹ Madhwesha Rao, PhD,¹
 Denise P. Yates, PhD,² Rob H. Ireland, PhD,³ Matthew Q. Hatton, MD,^{3,4}
 Bilal A. Tahir, PhD,^{1,3} Paul Ford, PhD,¹ Andrew J. Swift,¹ Rod Lawson, PhD,⁴
 Helen Marshall, PhD,¹ Guilhem J. Collier, PhD,¹ and Jim M. Wild, PhD^{1*}

Background: To support translational lung MRI research with hyperpolarized ^{129}Xe gas, comprehensive evaluation of derived quantitative lung function measures against established measures from ^3He MRI is required. Few comparative studies have been performed to date, only at 3T, and multisession repeatability of ^{129}Xe functional metrics have not been reported.

Purpose/Hypothesis: To compare hyperpolarized ^{129}Xe and ^3He MRI-derived quantitative metrics of lung ventilation and microstructure, and their repeatability, at 1.5T.

Study Type: Retrospective.

Population: Fourteen healthy nonsmokers (HN), five exsmokers (ES), five patients with chronic obstructive pulmonary disease (COPD), and 16 patients with nonsmall-cell lung cancer (NSCLC).

Field Strength/Sequence: 1.5T. NSCLC, COPD patients and selected HN subjects underwent 3D balanced steady-state free-precession lung ventilation MRI using both ^3He and ^{129}Xe . Selected HN, all ES, and COPD patients underwent 2D multislice spoiled gradient-echo diffusion-weighted lung MRI using both hyperpolarized gas nuclei.

Assessment: Ventilated volume percentages (VV%) and mean apparent diffusion coefficients (ADC) were derived from imaging. COPD patients performed the whole MR protocol in four separate scan sessions to assess repeatability. Same-day pulmonary function tests were performed.

Statistical Tests: Intermetric correlations: Spearman's coefficient. Intergroup/internuclei differences: analysis of variance / Wilcoxon's signed rank. Repeatability: coefficient of variation (CV), intraclass correlation (ICC) coefficient.

Results: A significant positive correlation between ^3He and ^{129}Xe VV% was observed ($r = 0.860$, $P < 0.001$). VV% was larger for ^3He than ^{129}Xe ($P = 0.001$); average bias, 8.79%. A strong correlation between mean ^3He and ^{129}Xe ADC was obtained ($r = 0.922$, $P < 0.001$). MR parameters exhibited good correlations with pulmonary function tests. In COPD patients, mean CV of ^3He and ^{129}Xe VV% was 4.08% and 13.01%, respectively, with ICC coefficients of 0.541 ($P = 0.061$) and 0.458 ($P = 0.095$). Mean ^3He and ^{129}Xe ADC values were highly repeatable (mean CV: 2.98%, 2.77%, respectively; ICC: 0.995, $P < 0.001$; 0.936, $P < 0.001$).

Data Conclusion: ^{129}Xe lung MRI provides near-equivalent information to ^3He for quantitative lung ventilation and microstructural MRI at 1.5T.

Level of Evidence: 3

Technical Efficacy: Stage 2

J. MAGN. RESON. IMAGING 2018;48:632–642.

The majority of hyperpolarized gas lung magnetic resonance imaging (MRI) studies that have been performed to date in patients with lung diseases have used ^3He gas, exploiting its intrinsically stronger MRI signal when

View this article online at wileyonlinelibrary.com. DOI: 10.1002/jmri.25992

Received Dec 12, 2017, Accepted for publication Feb 7, 2018.

*Address reprint requests to: J.M.W., Polaris, University of Sheffield, 18 Claremont Crescent, Sheffield, South Yorkshire, S10 2TA, UK.
 Email: j.m.wild@sheffield.ac.uk

From the ¹Academic Unit of Radiology, University of Sheffield, Sheffield, UK; ²Novartis Institutes for Biomedical Research, Cambridge, Massachusetts, USA; ³Academic Unit of Clinical Oncology, University of Sheffield, Sheffield, UK; ⁴Sheffield Teaching Hospitals NHS Foundation Trust, Sheffield, UK

This is an open access article under the terms of the Creative Commons Attribution License, which permits use, distribution and reproduction in any medium, provided the original work is properly cited.

compared to ^{129}Xe . However, recent years have seen an increase in ^{129}Xe lung MRI¹ studies in patients for assessment of lung ventilation,^{2–5} microstructure,^{6,7} and regional gas exchange⁸ with this naturally abundant isotope. This renewed interest is attributable to the relative scarcity of ^3He gas,⁹ and parallel developments in ^{129}Xe gas polarization technology^{10–13} and MRI pulse sequences¹⁴ that have helped bridge the gap in image quality due to the difference in gyromagnetic ratio between the two nuclei.

Previous comparisons of the sensitivity of ^3He and ^{129}Xe MRI for assessment of lung ventilation and microstructure have been reported in healthy subjects, former smokers,⁷ patients with chronic obstructive pulmonary disease (COPD),^{3,15} and asthma.¹⁶ Generally, lung ventilation and microstructural information of similar diagnostic quality has been obtained with the two nuclei, despite their different diffusivity in the lung airspaces. However, all of these reported studies were carried out at 3T, at relatively modest spatial resolution (15 mm and 30 mm slice thickness for ventilation and diffusion-weighted microstructural MRI, respectively), and at a single site.^{3,7,15,16} Magnetic susceptibility differences at 1.5T and 3T have been shown to have some impact on lung ventilation and diffusion-weighted microstructural MRI with both gases^{17,18}; however, quantitative information derived from ^3He and ^{129}Xe techniques at the most-reported field strength to date for lung MRI (1.5T) has yet to be systematically compared. This information is critical for multisite implementation and widespread clinical dissemination of ^{129}Xe MRI in the future.

In addition, future clinical use of ^{129}Xe will require quantitative data regarding the repeatability and robustness of associated MRI biomarkers of lung disease. The most commonly reported quantitative metrics of lung ventilation from conventional, static hyperpolarized gas images are percentage ventilated volume (VV%) and ventilation defect percentage (VDP = 100% – VV%). Same-day ^3He VDP measurements were reported to be highly repeatable at 3T in patients with COPD,^{19,20} while 1-week repeatability was relatively poorer. Good same-day and same-week repeatability of ^3He VV% has been reported in cystic fibrosis (CF) patients at 1.5T²¹ and 3T,²² respectively. One report of high same-session repeatability of ^{129}Xe VDP in healthy subjects and asthma patients has been published recently²³; however, multisession, multiday variability in quantitative lung ventilation metrics derived from ^{129}Xe MRI has not been assessed. Delivery of several doses of ^{129}Xe gas for ventilation imaging on the same/subsequent day to subjects with a variety of pulmonary conditions has been reported.^{2,24} However, the primary purpose of those studies was to assess safety and tolerability, and ventilation volume repeatability was not evaluated.

The global mean ^3He apparent diffusion coefficient (ADC) in the lung airspaces derived from diffusion-

weighted MRI is a well-established marker of alveolar microstructural change. Comprehensive investigations of same-session²⁵ and multiday²⁶ repeatability of mean ^3He ADC values have demonstrated a high intra-individual repeatability in healthy subjects and patients with emphysema. Furthermore, studies at 3T have highlighted a higher repeatability of ^3He ADC when compared to ^3He VDP in patients with COPD.^{19,20} However, to our knowledge, interscan repeatability of ^{129}Xe ADC has not been assessed to date. Evaluation of the repeatability of lung ventilation and microstructural metrics derived from ^{129}Xe MRI against ^3He MRI and pulmonary functional tests is therefore necessary to facilitate the clinical dissemination of these methods.

Taking the gaps in the literature discussed above into account, the purpose of this work was to evaluate the applicability and repeatability of quantitative metrics of ^{129}Xe ventilation and diffusion-weighted MRI as compared to the equivalent ^3He measurements made at a field strength of 1.5T.

Materials and Methods

Subjects

We present an analysis of MR data obtained from several distinct studies. Two groups of healthy nonsmokers: a) 11 participants (age = 43 ± 6 years), and b) three participants (age = 31 ± 4 years), all with no history of smoking or respiratory disorders; five ex-smokers with a pack history of ≥ 10 years and no history of respiratory disorders (age = 51 ± 2 years); five patients with COPD (GOLD stage: 3D [$n = 4$], 3B [$n = 1$]; age = 67 ± 7 years); and 16 patients with nonsmall-cell lung cancer (NSCLC) (age = 67 ± 12 years) were recruited for separate studies approved by the National Research Ethics Committee, with governance approval from the local National Health Service research committee. All subjects provided written informed consent. Patient demographics and pulmonary function test (PFT) results are summarized in Table 1. Subjects with a resting oxygen saturation of $< 90\%$, unstable cardiac disease, or (for NSCLC patients) comorbid conditions that precluded radiotherapy, were excluded.

MRI Technique

All subjects underwent MRI at 1.5T (GE HDx, GE Healthcare, Milwaukee, WI). Flexible quadrature radiofrequency coils were employed for transmission and reception of MR signals at the Larmor frequencies of ^3He and ^{129}Xe (Clinical MR Solutions, Brookfield, WI). ^3He and ^{129}Xe gas was polarized by collisional spin-exchange optical pumping, using a prototype commercial ^3He polarizer (MITI, Durham, NC) (average polarization $\sim 25\%$) and a home-built ^{129}Xe polarizer^{12,27} (average polarization $\sim 10\text{--}15\%$), respectively.

Patients with NSCLC and COPD, and three healthy nonsmokers (group b) underwent 3D lung ventilation MRI with a steady-state free precession (SSFP) sequence at breath-hold after inhalation of ^3He or ^{129}Xe gas.^{14,28} ^1H images of the thorax were also acquired for anatomical reference and calculation of total lung volume. As illustrated in Fig. 1 (right), ^1H images were acquired in both the same breath-hold²⁹ and a separate breath-hold as ^3He

TABLE 1. Summary of Subject Demographics, PFT Results, and ^3He and ^{129}Xe MRI Parameters

Parameter	Subject group				
	Healthy nonsmokers		Healthy ex-smokers	NSCLC patients	COPD patients
	a	b			
Age (yrs) (# of Subjects)	43.0 ± 6.4 (6M, 5F)	30.7 ± 3.5 (3M)	51.0 ± 2.3 (3M, 2F)	66.9 ± 12.0 (10M, 6F)	67.4 ± 6.5 (2M, 3F)
FEV ₁ (%-pred)	101.0 ± 12.5	92.6 ± 15.9	94.9 ± 9.8	72.7 ± 25.0	38.0 ± 6.6
FEV ₁ /FVC (%)	77.1 ± 7.2	77.0 ± 7.6	75.1 ± 13.2	57.1 ± 16.5	29.7 ± 5.9
D _{LCO} (%-pred)	89.6 ± 17.8	102.3 ± 9.3	103.5 ± 16.2	56.6 ± 31.0	42.5 ± 32.4
^3He VV%	—	98.4 ± 0.60	—	79.6 ± 11.7	71.4 ± 7.8
^{129}Xe VV%	—	96.6 ± 0.32	—	70.8 ± 13.3	59.8 ± 10.4
^3He ADC _{glob} (cm ² ·s ⁻¹)	0.190 ± 0.017	—	0.211 ± 0.022	—	0.432 ± 0.127
^{129}Xe ADC _{glob} (cm ² ·s ⁻¹)	0.038 ± 0.003	—	0.043 ± 0.004	—	0.073 ± 0.019

FEV₁ = forced expiratory volume in 1 second; FVC = forced vital capacity; D_{LCO} = diffusing capacity of the lung for carbon monoxide; %-pred = PFTs expressed as a percentage of a predicted value, based on the subject's age, height, and other demographic factors.

ventilation images (same breath-hold for ease of image registration; separate breath-hold in case same breath-hold acquisition failed or could not be registered). Due to the length of the ^{129}Xe ventilation imaging breath-hold, ^1H images were acquired in a separate breath-hold. VV% was derived by segmentation (and registration if required) of paired sets of hyperpolarized gas and corresponding ^1H images as described previously²⁸ (VV% = volume of

"ventilated" regions from segmentation of hyperpolarized gas images / total lung volume from segmentation of ^1H images). In addition to calculation of VV%, images were qualitatively assessed for size and number of ventilation defects (regions of unventilated signal, defined as falling below 2 standard deviations of the noise) and signal heterogeneity in ventilated areas. Hyperpolarized gas and ^1H pulse sequence parameters are listed in Table 2. In each

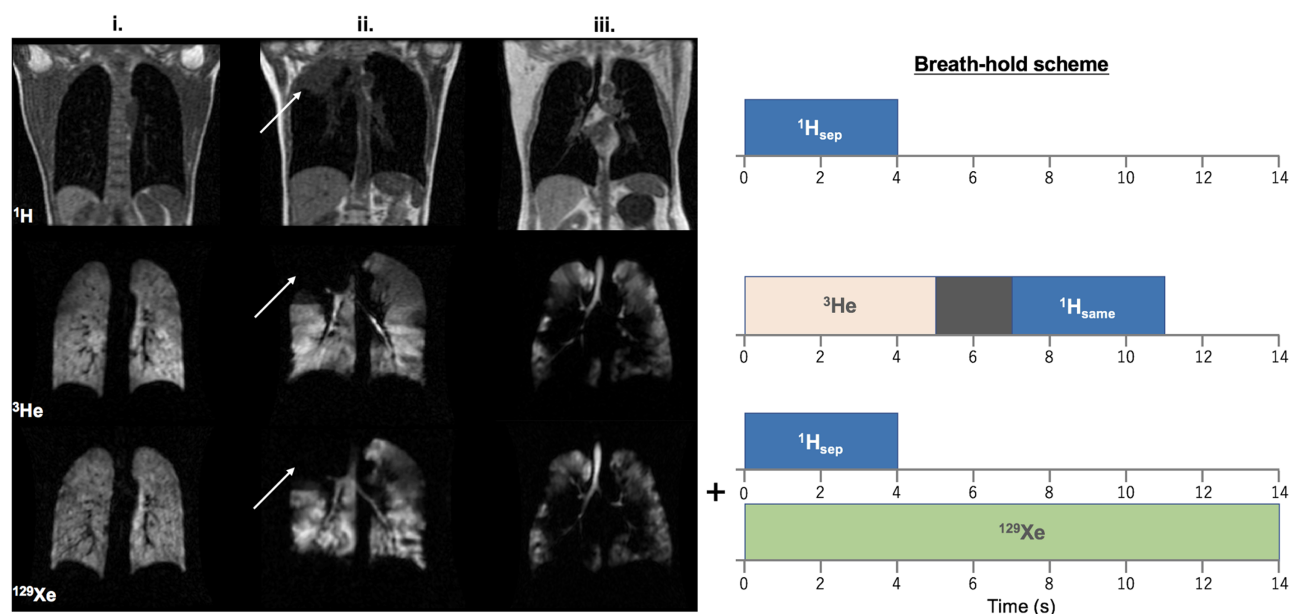


FIGURE 1: Left: Comparison of ^3He and ^{129}Xe MR ventilation images of i. a healthy nonsmoker (group b), ii. a patient with NSCLC (white arrows indicate the location of a lesion), and iii. a patient with COPD. (Note: The slice thickness of ^3He images is half that of ^{129}Xe images; see Table 2). Right: Corresponding breath-hold scheme for ventilation imaging scans. Scans were acquired in the order shown, with a change of RF coil and repositioning of the patient between ^3He and ^{129}Xe scans.

TABLE 2. Summary of MR Pulse Sequence Acquisition Parameters

Metric	^3He VV%		^{129}Xe VV%		^3He ADC	^{129}Xe ADC
	^3He 3D SSFP	^1H 3D SPGR	^{129}Xe 3D SSFP	^1H 3D SPGR	DW 2D SPGR	DW 2D SPGR
FOV (cm)	~40	~40	~40	~40	~40	~40
Phase FOV	0.8	1.0	0.8	1.0	0.75	0.75
Matrix	100 × 80	100 × 100	100 × 80	100 × 100	64 × 64	64 × 48
Pixel size (mm)	4 × 4	4 × 4	4 × 4	4 × 4	6.25 × 6.25	6.25 × 8.33
# of slices	~48	~48	~24	~24	5	4
Slice thickness (mm)	5	5	10	10	15 (10 mm gap)	15 (10 mm gap)
Flip angle (°)	9	5	9/10 ^a	5	4.8	6.7
TE/TR (msec)	0.6/1.9	0.6/1.9	2.2/6.7	0.6/1.9	4.8/10.0	12.5/27.0
BW(kHz)	±83.3	±83.3	±8	±83.3	±31.25	±2
Gas dose (ml)	200	N/A	600	N/A	300	600
Breath-hold (s)	5	4	14	4	16	16
	~14 (^3He +gap+ ^1H)		—	—	—	—
Δ (ms)	—	—	—	—	1.6 ($\tau=0.3$; $\delta=1.0$; X=0)	5.0 ($\tau=0.3$; $\delta=3.0$; X=1.4)
N_D	—	—	—	—	6	4
G_m (mT.m ⁻¹)	—	—	—	—	31.6	32.2
$b_{1,2}$ (s.cm ⁻²)	—	—	—	—	0; 1.6	0; 8.0

SSFP: steady-state free precession; SPGR: spoiled gradient echo; FOV: field of view; TE: echo time; TR: repetition time; BW: bandwidth; Δ : diffusion time, τ : ramp time, δ : plateau time; X: separation of gradient lobes; N_D : number of diffusion-weighted interleaves; G_m : maximum gradient amplitude; $b_{1,2}$: b values of first two interleaves.
FOV and ventilation # of slices were increased if necessary to cover the whole lungs of larger patients.
^aFlip angle was 9° for COPD patients, 10° for NSCLC patients.

case, a dose of ^3He (99.25% of 100% ^3He isotope, 0.75% N_2) or 129-enriched xenon (86% ^{129}Xe) gas was balanced to 1 L with N_2 in a Tedlar bag and inhaled via a sterilized air filter. Prior to image acquisition, subjects inhaled from functional residual capacity (FRC) after a period of steady breathing. Target inhaled gas doses were achieved to within a tolerance of ± 10 mL for ^3He and ± 20 mL for ^{129}Xe . Images with a signal-to-noise ratio (SNR) of <5 were not included in quantitative analysis. This threshold was determined by quantitative evaluation of the effect of SNR on ventilation heterogeneity³⁰ by incrementally adding noise to high SNR ventilation images.

Healthy nonsmokers (group a), ex-smokers, and COPD patients underwent 2D multislice ^3He and ^{129}Xe diffusion-weighted lung MRI to acquire ADC maps of the lungs. ADC values were calculated from the first two interleaves of a multiple b -value 2D diffusion-weighted spoiled gradient echo sequence. Acquisition parameters and bipolar diffusion gradient timing parameters are summarized in Table 2. Gradients were designed to achieve comparable diffusion weighting for the two nuclei, and slice locations were matched (with an additional anterior slice for ^3He acquisitions). The same SNR threshold as ventilation imaging

was applied to diffusion-weighted MRI data. Note: Healthy non-smokers (group a) and ex-smokers did not undergo ventilation imaging in this study. Likewise, patients with NSCLC and healthy group b did not undergo diffusion-weighted MRI.

Patients with COPD underwent the complete MR protocol on four separate scan sessions in total: twice on day 1; once on day 2; and once 2 weeks after day 1, to assess the repeatability of ^3He and ^{129}Xe metrics.

Pulmonary Function Testing

PFTs, including the diffusing capacity of the lung for carbon monoxide (D_{LCO}) and spirometry, were performed by each COPD patient, once on the same day as each MR session (three times in total, always following MRI). Healthy nonsmokers and ex-smokers performed the same tests immediately after their single-timepoint diffusion-weighted MR scans, and NSCLC patients performed PFTs within ± 1 week of MRI.

Statistical Analysis

VV% and global mean ADC (ADC_{glob}) values derived from ^3He and ^{129}Xe MRI were compared for differences in each metric

between two, or more than two, *subject groups* with conventional *t*-tests or analyses of variance (ANOVA), respectively. Differences in metrics derived between *gas nuclei* were analyzed using Wilcoxon signed rank tests. Spearman's rank correlation coefficients were derived to quantify the relationship between ^3He and ^{129}Xe datasets, and Bland–Altman analysis was used to visualize systematic differences in VV% between the two nuclei. MRI metrics were compared and correlated against PFT results by calculating Spearman's rank coefficients. The mean of repeated measurements from each COPD patient was used to represent a single datapoint for the above statistical tests.

Where repeatability data were available, the coefficient of variation (CV) of each parameter was calculated as the ratio of the standard deviation (SD) to the mean over all repeated measurements, expressed as a percentage. In addition, two-way mixed intraclass correlation (ICC) coefficients were calculated for absolute agreement between repeat measurements. Statistical analyses were performed using IBM SPSS Statistics (v. 23, Armonk, NY) and R (R3.4, R Foundation for Statistical Computing, Vienna, Austria), and statistical significance level was set to $P < 0.05$.

Results

Imaging Data Quality

From the healthy nonsmokers cohort, ^{129}Xe diffusion-weighted MR images from one subject exhibited insufficient SNR for accurate calculation of ADC maps. From the COPD cohort, one ^3He and one ^{129}Xe ADC dataset, and two ^3He and two ^{129}Xe VV% datasets (each out of a total of 20 datasets for each nucleus, each metric) were either not successfully acquired or image SNR was unsatisfactory. From the NSCLC patient cohort, one ^3He dataset and one ^1H dataset was not acquired successfully, and two ^{129}Xe datasets showed low SNR.

All other recorded data were of sufficient SNR for analysis: ie, for ^3He , $>95\%$ of ADC data and $>90\%$ of VV% data were acceptable; for ^{129}Xe , 95% of ADC data and $>85\%$ of VV% data were acceptable. All gas doses were well-tolerated and no significant side effects or adverse events were reported. Mean MR parameters and PFT results are shown in Table 1.

Ventilation Imaging

Representative ^3He and ^{129}Xe coronal ventilation images and corresponding structural ^1H images from patients with NSCLC and COPD are shown in Fig. 1 (left), alongside images from a healthy nonsmoker. Considerable ventilation abnormalities were observed in patients with NSCLC, with most patients exhibiting a heterogeneous distribution of ventilated airspaces and complete absences of ventilation in the region of the lung associated with malignancies (as identified on structural ^1H MRI). Severe ventilation defects were detected in most COPD patients, and entire lobes of the lungs were often observed to be completely unventilated.

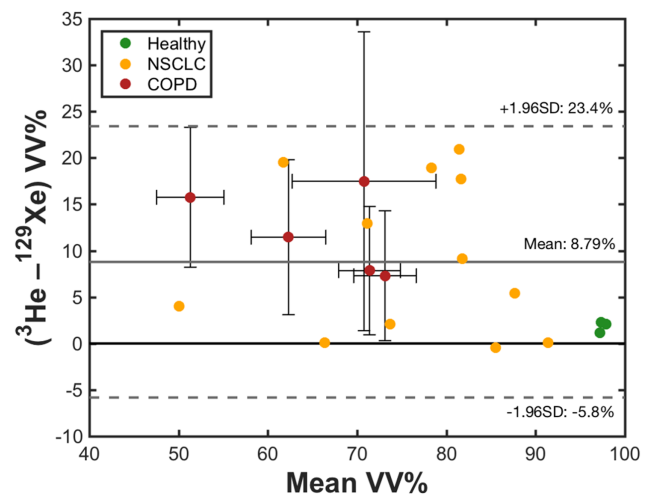


FIGURE 2: Bland–Altman analysis of ^3He and ^{129}Xe VV% values in patients with NSCLC and COPD and healthy nonsmokers group b. The solid gray line indicates the mean difference (bias) between ^3He and ^{129}Xe VV%, and dashed lines represent ± 1.96 standard deviations from the mean. Datapoints and error bars for COPD patients denote intrasubject means and standard deviations of repeated acquisitions, respectively.

By pooling data from healthy nonsmokers (group b) and patients with NSCLC and COPD, a significant positive correlation between ^3He and ^{129}Xe VV%, was identified (Spearman's correlation coefficient, $r = 0.860$, $P < 0.001$). Derived VV% values were larger on average for ^3He when compared with ^{129}Xe (mean over all healthy group b, NSCLC, and COPD subjects); $P < 0.001$ (Wilcoxon signed rank) and qualitatively, typically larger and more numerous ventilation defects could be observed in ^{129}Xe images. A Bland–Altman plot of the systematic differences between ^3He and ^{129}Xe VV% is shown in Fig. 2, indicating a bias of $+8.79\%$ towards higher ^3He VV%. Analyzing data from COPD and NSCLC patients separately, intragroup correlations between ^3He and ^{129}Xe VV% were statistically significant for NSCLC patients ($r = 0.657$, $P = 0.024$) but not COPD patients ($r = 0.700$, $P = 0.233$). Additionally, ^3He VV% values were found to be higher than ^{129}Xe VV% values when COPD ($P = 0.063$, close to significant) and NSCLC ($P = 0.002$, significant) patient data were analyzed separately. There were no significant differences in either mean ^3He VV% ($P = 0.095$) or mean ^{129}Xe VV% ($P = 0.085$) values between the two patient groups, although the VV% trended to be lower in COPD patients compared with NSCLC patients.

Diffusion-Weighted Imaging

Examples of ^3He and ^{129}Xe ADC maps obtained from a healthy nonsmoker and a patient with COPD are shown in Fig. 3. ADC_{glob} values of both nuclei were significantly elevated in COPD patients when compared to both healthy nonsmokers (group a) and ex-smokers: ^3He $\text{ADC}_{\text{glob}} = 0.432 \pm 0.127 \text{ cm}^2 \cdot \text{s}^{-1}$ in COPD patients, $0.211 \pm 0.022 \text{ cm}^2 \cdot \text{s}^{-1}$ in

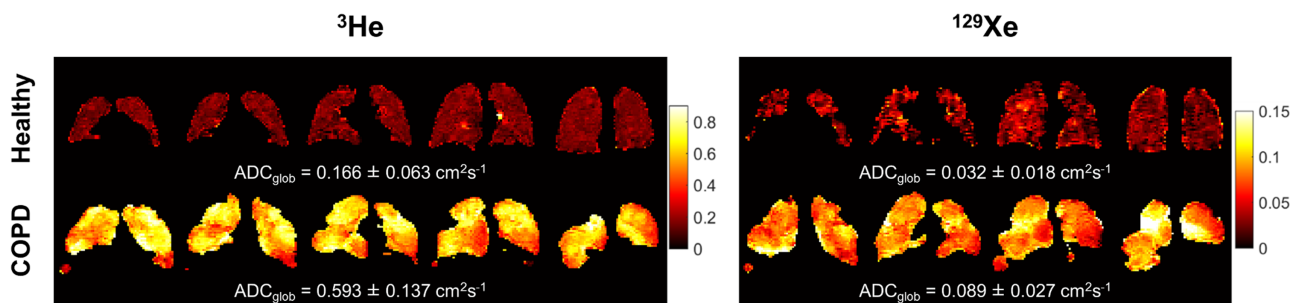


FIGURE 3: Representative dataset of ^3He and ^{129}Xe ADC maps obtained from a healthy nonsmoker (group a) and a patient with COPD. The mean ADC over all slices is quoted underneath each dataset.

ex-smokers ($P=0.036$ vs. COPD patients) and $0.190 \pm 0.017 \text{ cm}^2 \cdot \text{s}^{-1}$ in healthy nonsmokers ($P=0.028$ vs. COPD patients); mean ^{129}Xe $\text{ADC}_{\text{glob}} = 0.073 \pm 0.019 \text{ cm}^2 \cdot \text{s}^{-1}$ in COPD patients, $0.042 \pm 0.004 \text{ cm}^2 \cdot \text{s}^{-1}$ in ex-smokers ($P=0.045$ vs. COPD patients) and $0.038 \pm 0.003 \text{ cm}^2 \cdot \text{s}^{-1}$ in healthy nonsmokers ($P=0.029$ vs. COPD patients). Ex-smoker and healthy nonsmoker ADC_{glob} values were statistically indistinguishable; $P=0.214$ and $P=0.114$ for ^3He and ^{129}Xe data, respectively.

A strong positive correlation between ^3He and ^{129}Xe ADC_{glob} was found when pooling data from healthy nonsmokers group a, ex-smokers and COPD patients together (Fig. 4: Spearman's $r=0.922$, $P<0.001$). Analyzing the three subject groups separately, significant correlations between ^3He and ^{129}Xe ADC_{glob} were observed for each of the three groups ($P<0.05$).

MR Metrics vs. PFTs

A summary of the statistical analyses of relationships between MR metrics and PFTs is presented in Table 3. Both ^3He and ^{129}Xe VV% exhibited significant correlations with FEV_1 and FEV_1/FVC at $P<0.001$ (except ^{129}Xe VV% vs. FEV_1 , $P<0.05$ significance level). Correlations of

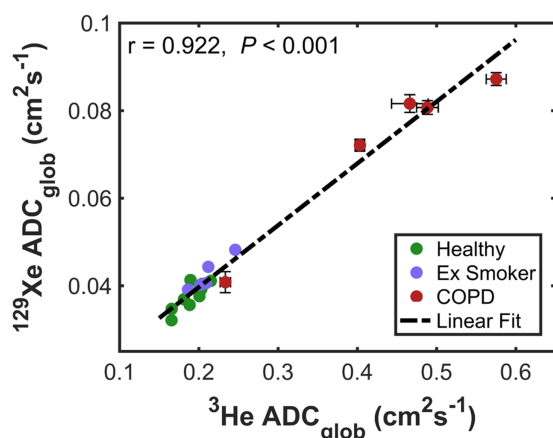


FIGURE 4: Correlation between mean ^3He and ^{129}Xe ADC_{glob} in healthy nonsmokers (group a), ex-smokers, and patients with COPD, with associated Spearman's correlation coefficient (r) and P value of statistical significance. The dashed line represents a linear fit to the data and error bars represent the standard deviation of repeated scans for each COPD patient.

VV% values derived from both nuclei with D_{LCO} were relatively weaker, although still significant at the $P<0.05$ level. Note: One significant outlying datapoint from a patient with NSCLC with %-predicted spirometry $\sim 90\%$ but low VV% values, $\sim 50\%$ for both nuclei, was excluded from the analysis presented in Table 3. When these outlying data were included in the analysis, the correlation statistics were severely affected; correlations of VV% with D_{LCO} were no longer significant ($P>0.05$) and all other correlations were significant at the $P<0.05$ level, rather than $P<0.001$ (Table 3 caption).

ADC_{glob} values also showed strong correlations with PFTs; notably, correlations of ^3He ADC_{glob} with both FEV_1 and FEV_1/FVC were significant at the $P<0.001$ level, while correlations with D_{LCO} were significant at the $P<0.05$ level (Table 3). Similarly, correlations of ^{129}Xe ADC_{glob} with FEV_1 were significant to $P<0.001$, and correlations with FEV_1/FVC and D_{LCO} were significant to $P<0.05$.

Repeatability

In COPD patients, both ^3He and ^{129}Xe ventilation images appeared qualitatively similar (in terms of visual ventilation defect prevalence and ventilation homogeneity) at each of the four scan timepoints, as shown for a representative example in Fig. 5. Mean CV values of ^3He and ^{129}Xe VV% between all repeated scans were 4.08% and 13.01%, respectively (Table 4). According to ICC analysis, both ^3He VV% (ICC coefficient 0.541, $P=0.061$) and ^{129}Xe VV% (coefficient 0.458, $P=0.095$) repeatability—calculated by considering data from all scan timepoints—was classified as just beyond the 95% confidence level. The CV of ^3He VV% was comparable to that of PFTs, while the ^{129}Xe VV% CV was higher.

Good agreement in the appearance of both ^3He and ^{129}Xe ADC maps was observed for each scan timepoint, as illustrated in Fig. 6. ^3He and ^{129}Xe ADC_{glob} values were highly repeatable over all scan sessions, with ICC coefficients for interscan agreement (0.995 and 0.936 for ^3He and ^{129}Xe , respectively) significant at the $P<0.001$ level, and mean CV values of $<3\%$ in both cases (see Table 4).

TABLE 3. Correlations Between MRI-Derived ^3He and ^{129}Xe VV% and ADC Measurements and PFTs

r (P)	^3He ADC	^{129}Xe ADC	^3He VV%	^{129}Xe VV%
D_{LCO} (%-pred)	-0.537 (0.018 ^a)	-0.628 (0.005 ^a)	0.524 ^c (0.019 ^a)	0.476 ^c (0.035 ^a)
FEV_1 (%-pred)	(-0.724 <0.001 ^b)	-0.834 (<0.001 ^b)	0.732 (<0.001 ^b)	0.648 (0.002 ^a)
FEV_1/FVC	-0.747 (<0.001 ^b)	-0.672 (0.001 ^a)	0.819 (<0.001 ^b)	0.744 (<0.001 ^b)

^aCorrelations at the statistical significance level of $P < 0.05$.
^bCorrelations at the statistical significance level of $P < 0.001$.
^cResults of correlating VV% values with PFTs represent the statistics obtained when outlying data associated with one NSCLC patient was excluded. When this data-point was included, the correlation coefficients (P values) for VV% altered as follows: ^3He , 3 rows: 0.432 (0.052); 0.592 (0.005^a); 0.559 (0.012^a); ^{129}Xe , 3 rows: 0.387 (0.084); 0.531 (0.012^a); 0.529 (0.015^a).
 %-pred: %-predicted pulmonary function test result.

ICC coefficients and CVs of ADC_{glob} values were comparable to those of FEV_1 and FEV_1/FVC , and considerably less than those of D_{LCO} and VV%.

Discussion

This work indicates that ^{129}Xe lung MRI can provide equivalent regional information on lung ventilation and microstructure to ^3He MRI at to-date the most-reported field strength for lung MRI, 1.5T. Specifically, we demonstrated a clear agreement between ^{129}Xe ventilation and diffusion MRI measurements and ^3He equivalent measurements; these findings substantiate previous work from the Robarts group that was performed at 3T with lower spatial resolution imaging.^{3,15,16} We also quantified the repeatability of ^{129}Xe ventilation and diffusion-weighted MRI metrics against ^3He equivalent measurements in COPD patients.

^3He and ^{129}Xe VV% correlated strongly, with a positive bias towards increased VV% for ^3He . Discrepancies can

likely be attributed to differences in image slice thickness, gas polarization, and the fundamental properties of the gases as discussed below. The generally lower VV% of ^{129}Xe may be explained by the ~ 5 -fold lower diffusion coefficient of xenon in air (as confirmed by the mean ADCs of the two gases measured in healthy lungs here), and the resulting slower penetration of partially obstructed airways, although the relatively lower mean SNR of ^{129}Xe ventilation images may also contribute to this observation. In patients with severe disease, partially obstructed airways may cause an accentuation of this diffusion-related effect, leading to observation of further ventilation abnormalities with ^{129}Xe when compared with ^3He . We note that a time-dependent diffusive effect of delayed filling of ventilation defects and collateral ventilation has been observed in COPD patients by ^3He MRI,³¹ but the equivalent measurements has not yet been reported for ^{129}Xe . A reduced VV% for ^{129}Xe when compared with ^3He was also reported previously at 3T^{3,16}

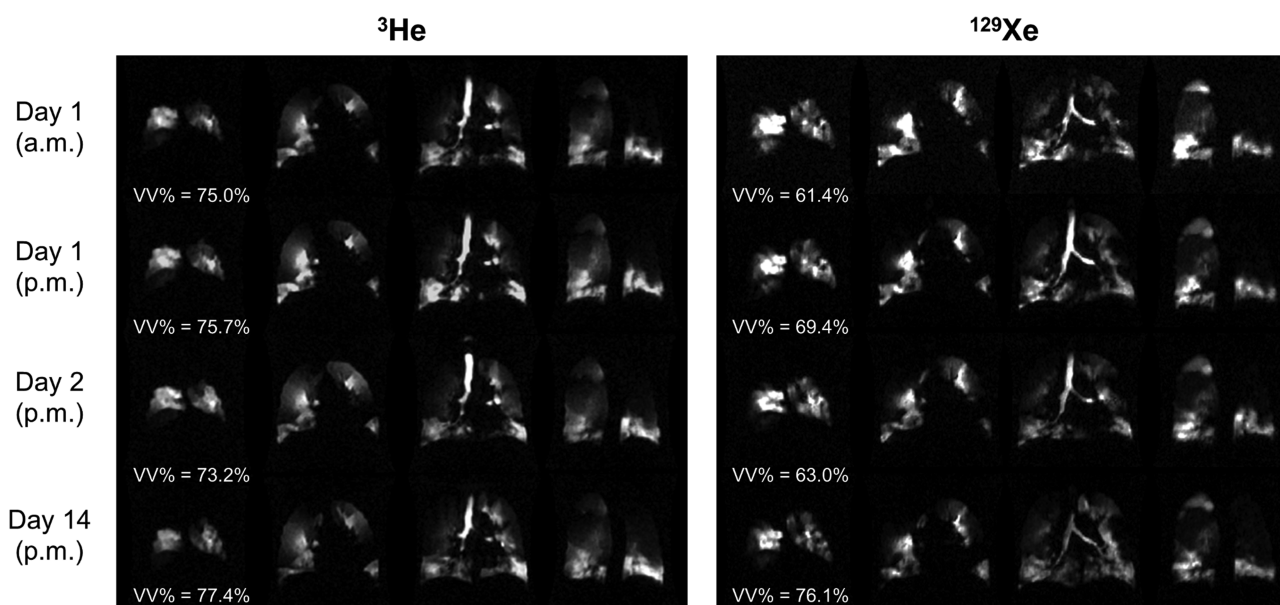


FIGURE 5: Selected ^3He and ^{129}Xe ventilation image slices acquired at each of the four scan timepoints of the repeatability study from a COPD patient. Calculated ventilated volume percentages (VV%) are quoted underneath each respective set of images.

TABLE 4. Repeatability of PFTs and MRI Metrics in Patients With COPD

	ICC (<i>P</i> value)	CV mean (%)	CV range (%)
FEV ₁ (%-pred)	0.934 (<0.001 ^b)	4.22	2.16–6.35
FEV ₁ /FVC	0.987 (<0.001 ^b)	2.34	1.49–3.80
D _{LCO} (%-pred)	0.992 (<0.001 ^b)	8.73	3.91–16.15
^3He VV%	0.541 (0.061)	4.08	2.21–8.86
^{129}Xe VV%	0.458 (0.095)	13.01	9.62–25.28
^3He ADC _{glob}	0.995 (<0.001 ^b)	2.98	1.48–5.61
^{129}Xe ADC _{glob}	0.936 (<0.001 ^b)	2.77	1.68–5.88

ICC = intraclass correlation coefficient; CV = coefficient of variation.
^aStatistical significance level of $P < 0.05$.
^bStatistical significance level of $P < 0.001$.

and attributed to lower diffusivity. Furthermore, systematically higher absolute ventilated volumes have been reported for ^3He when compared with ^{129}Xe at 3T,¹⁵ wherein it was suggested that ^3He has a higher propensity to flow through collateral channels in COPD patients. Nevertheless, this property of ^{129}Xe could prove useful in the assessment of early (ie, small-scale) structural abnormalities of distal airways and lung parenchyma in a variety of pulmonary diseases, provided that equivalent image SNR and spatial resolution can be achieved as that of ^3He MRI.

The lower CV values (and higher ICC coefficients) of ^3He VV% when compared with ^{129}Xe VV% are likely attributable to the generally lower and more variable SNR of ^{129}Xe images acquired at the time of the study (mean \pm standard deviation of SNR over all NSCLC and COPD

patients: 23.6 ± 16.8 for ^{129}Xe ; 30.6 ± 10.8 for ^3He), and the differences in lung inflation level in some cases between ^{129}Xe and anatomical ^1H images acquired in a separate breath-hold.²⁸ As mentioned in the Materials and Methods, polarization levels, and thus image SNR, affect the ventilation heterogeneity and therefore images with low SNR (<5) can significantly distort the physiological interpretation of the data. The relatively lower SNR may be explained by the fact that a prototype ^{129}Xe polarizer (producing ^{129}Xe polarization ~ 10 –15%) was used for most ^{129}Xe experiments in this work.¹² We have since developed and optimized a clinical-scale polarizer capable of rapidly producing ^{129}Xe polarized to $\sim 40\%$, which will enable improved ^{129}Xe image SNR in future studies.²⁷ Nevertheless, the CV of ^{129}Xe VV% is severely biased by an outlying subject (CV of

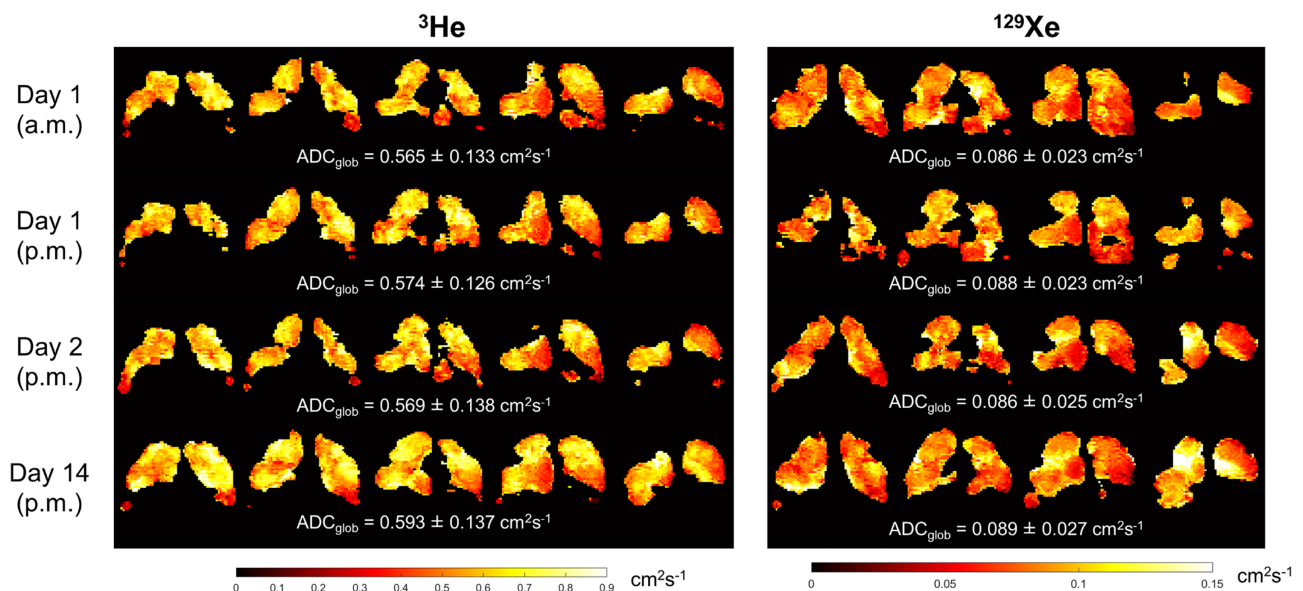


FIGURE 6: Representative ^3He and ^{129}Xe ADC maps acquired at each of the four scan timepoints of the repeatability study from a COPD patient. Global mean ADC values (ADC_{glob}) are quoted underneath each respective set of maps.

25%); the CV in all other COPD patients was $\sim 10\%$. The ^{129}Xe images from the first scan session in this outlying subject were excluded from analysis because of insufficient SNR. Despite this observation, no other metrics showed abnormally high CV for that patient and no differences in the patient's clinical status were noted.

The high regional heterogeneity of COPD may explain the increased CV of VV% when compared with ADC_{glob} (ADC maps are of lower resolution than ventilation images), although we note that, qualitatively, the prominent areas of ventilation defect were observed repeatedly over scan sessions. Furthermore, the variability of bronchodilator therapy applied on a day-to-day basis will potentially impact VV% more severely than ADC. Nonetheless, both ^3He and ^{129}Xe VV% CV values calculated from COPD patient data are similar to week-to-week percentage variability in FEV_1 and D_{LCO} ,³² and same-day ^3He VV% variability in pediatric CF patients,²¹ as reported earlier, although poorer than or comparable to the repeatability of PFTs measured in the present work. Our ICC values for ^{129}Xe VV% are considerably lower than same-session (10 minutes apart) ^{129}Xe VDP ICCs reported by Ebner et al²³; however, the differences can potentially be explained by the fact that in that work, patients did not leave the scanner between scans, no multisession/multiday data were recorded, and the number of patients was significantly higher than in the present work. Otherwise, the results of ^{129}Xe VV% and ADC repeatability have, to our knowledge, not been previously reported, and hence our measurements can only be assessed against literature data for equivalent ^3He measurements. Resolution of some of the issues discussed herein, including utilization of the higher performance polarizer, should lead to improvements in the repeatability of ^{129}Xe VV% to a similar level as ^3He , thus facilitating translation to large-scale clinical studies.

Typically, lower imaging bandwidths and larger diffusion gradients are required for ^{129}Xe when compared with ^3He lung MRI, necessitating longer breath-hold times or lower spatial resolutions. Additionally, until recently, ^{129}Xe polarizer performance has not been adequate to overcome the inherent MR signal disadvantages compared with ^3He . As such, a compromise was reached in this work, such that the in-plane resolution of ^{129}Xe ventilation imaging acquisitions matched that of ^3He , but the slice resolution was halved. Developments in compressed sensing (CS) and parallel imaging acquisition strategies for accelerated imaging^{33,34} should help permit equivalent, isotropic resolution ^{129}Xe , and ^3He ventilation imaging within a clinically feasible breath-hold in the near future, and facilitate same-breath ^{129}Xe and ^1H imaging for improved ^{129}Xe ventilation volumetry. Moreover, it has recently been demonstrated that 3D multiple b -value diffusion-weighted CS-based acquisition strategies for whole-lung morphometric analysis developed

for diffusion-weighted ^3He MRI³⁵ are readily transferable to ^{129}Xe .³⁶ Although the through-plane ^{129}Xe ventilation and diffusion image resolution in this work is already superior to previous reports at 3T, the adoption of CS methods for both applications should enable these resolution limits to be pushed further towards those attainable with ^3He .

Mean ADC_{glob} values of both nuclei exhibited excellent correlation with each other and high repeatability in COPD patients, with comparable or lower interscan CVs than conventional PFTs, suggesting that ^{129}Xe diffusion-weighted MR has approximately equal sensitivity to ^3He for quantitative assessment of lung microstructural changes, and sufficient reliability for routine clinical application.

The observation of elevated ADC_{glob} in COPD patients agrees with previous reports for both ^3He ^{3,26} and ^{129}Xe ,^{6,7} and has been well characterized. Similarly, increased ADC_{glob} in subjects with smoking history is consistent with previous observations,⁷ although the ^{129}Xe b -values used in those works differ from this work. As a consequence of the non-Gaussian phase dispersion of the ^3He and ^{129}Xe diffusion regime experienced in the lungs, ADC_{glob} exhibits some variation with b -value,³⁷ which constrains the validity of interstudy comparisons. As such, we recommend that for ease of implementation and comparison across sites, a standardized b -value and diffusion time should be adopted for ^{129}Xe diffusion-weighted MRI, similar to the value of $1.6 \text{ s}\cdot\text{cm}^{-2}$ now widely used for ^3He .

CV values of both ^3He and ^{129}Xe ADC_{glob} are less than those of previously reported same-day variability in FEV_1 ,³² and substantially lower than measured variability in D_{LCO} ($\sim 9\%$)³⁸. D_{LCO} is perhaps the most relevant PFT to compare with ADC, since both measurements rely on gas diffusion within the alveoli, albeit for studying different lung physiology. Thus, the observed repeatability is extremely promising for advancing ^{129}Xe diffusion-weighted MRI to large-scale multisite trials with the goal of routine clinical implementation. Additionally, our reported CV values of both ^3He and ^{129}Xe ADC_{glob} are less than ^3He ADC CVs reported for healthy subjects and patients with emphysema at 1.5T,²⁶ and are comparable to ^3He CVs measured at 3T.²⁰

The design of the present study has some limitations that could be effectively resolved in future studies. Although a reasonable number of patients were included in this study (37 in total), repeatability experiments were only performed on five patients and, thus, a follow-up comprehensive, repeatability-specific study is required with an increased number of subjects, including both patients and volunteers. In such a study, it may be statistically meaningful to distinguish same-day from 2-week repeatability, and therefore better identify potential sources of physiological variability between different scan sessions. Due to a few missing data-sets, the current data is insufficient in quantity for such

statistically sound intertimepoint repeatability analysis; hence, the repeatability was only analyzed over all scan sessions. Data regarding day-to-day and week-to-week repeatability is critical for understanding the natural physiological variability in VV% and ADC_{glob} in patients and discriminating this from measurement uncertainty.

In conclusion, the findings reported herein demonstrate that ^{129}Xe is approaching readiness as a clinically viable alternative to ^3He for quantitative lung ventilation and microstructural MRI studies. For future dissemination and multisite cross-platform clinical trials, the fact that our results agree with many of the trends seen in prior studies that benchmarked ^3He and ^{129}Xe MRI measurements at 3T is encouraging. Although quantitative measurements of ventilation and ADC will be biased by magnetic susceptibility effects at the two field strengths, we believe that equivalent functional information can be achieved with both gases at both field strengths. In addition, the high repeatability of both ^3He and ^{129}Xe ADC observed here is perhaps the most convincing evidence to date that ^{129}Xe ADC imaging has developed into a robust microstructural imaging methodology. Moreover, this report builds upon previous measurements at 3T in terms of improved spatial resolution of ^{129}Xe imaging, and the realization of 3D DW-MRI with both nuclei^{35,36} is extremely promising for further validation and clinical application in the near future. The preliminary assessment of the repeatability of ^{129}Xe ventilation and diffusion MRI biomarkers addresses a gap in knowledge that was not considered prior to this work and paves the way for further, more comprehensive multisite repeatability studies.

Conflict of Interest

Dr. Yates was involved in the study design and imaging protocol for the COPD imaging metric repeatability study. She is part of the Novartis imaging biomarker team and this work was not related to a clinical trial of a therapeutic.

References

- Mugler JP, Altes TA. Hyperpolarized ^{129}Xe MRI of the human lung. *J Magn Reson Imaging* 2013;313–331.
- Driehuis B, Martinez-Jimenez S, Cleveland ZI, et al. Chronic obstructive pulmonary disease: Safety and tolerability of hyperpolarized ^{129}Xe MR imaging in healthy volunteers and patients. *Radiology* 2012;262:279–289.
- Kirby M, Svenningsen S, Owrangi A, et al. Hyperpolarized ^3He and ^{129}Xe MR imaging in healthy volunteers and patients with chronic obstructive pulmonary disease. *Radiology* 2012;265:600–610.
- Thomen RP, Walkup LL, Roach DJ, Cleveland ZI, Clancy JP, Woods JC. Hyperpolarized ^{129}Xe for investigation of mild cystic fibrosis lung disease in pediatric patients. *J Cyst Fibros* 2017;16:275–282.
- Virgincar RS, Cleveland ZI, Sivaram Kaushik S, et al. Quantitative analysis of hyperpolarized ^{129}Xe ventilation imaging in healthy volunteers and subjects with chronic obstructive pulmonary disease. *NMR Biomed* 2013;26:424–435.
- Kaushik SS, Cleveland ZI, Cofer GP, et al. Diffusion-weighted hyperpolarized ^{129}Xe MRI in healthy volunteers and subjects with chronic obstructive pulmonary disease. *Magn Reson Med* 2011;65:1155–1165.
- Kirby M, Ouriadov A, Svenningsen S, et al. Xe magnetic resonance imaging apparent diffusion coefficients: Physiological relevance on older never- and exsmokers. *Physiol Rep* 2014;2:e12068.
- Qing K, Ruppert K, Jiang Y, et al. Regional mapping of gas uptake by blood and tissue in the human lung using hyperpolarized xenon- ^{129}Xe MRI. *J Magn Reson Imaging* 2014;39:346–359.
- Shea DA. The helium-3 shortage: Supply, demand, and options for Congress. *Congr Res Serv Rep Congr* 2010.
- Hersman FW, Ruset IC, Ketel S, et al. Large production system for hyperpolarized ^{129}Xe for human lung imaging studies. *Acad Radiol* 2008;15:683–692.
- Nikolaou P, Coffey AM, Walkup LL, et al. Near-unity nuclear polarization with an open-source ^{129}Xe hyperpolarizer for NMR and MRI. *Proc Natl Acad Sci U S A* 2013;110:14150–14155.
- Norquay G, Parnell SR, Xu X, Parra-Robles J, Wild JM. Optimized production of hyperpolarized ^{129}Xe at 2 bars for in vivo lung magnetic resonance imaging. *J Appl Phys* 2013;113:44908.
- Six JS, Hughes-Riley T, Stupic KF, Pavlovskaya GE, Meersmann T. Pathway to cryogen free production of hyperpolarized krypton-83 and xenon- ^{129}Xe . *PLoS One* 2012;7:e49927.
- Stewart NJ, Norquay G, Griffiths PD, Wild JM. Feasibility of human lung ventilation imaging using highly polarized naturally abundant xenon and optimized three-dimensional steady-state free precession. *Magn Reson Med* 2015;74:346–352.
- Kirby M, Svenningsen S, Kanhere N, et al. Pulmonary ventilation visualized using hyperpolarized helium-3 and xenon- ^{129}Xe magnetic resonance imaging: Differences in COPD and relationship to emphysema. *J Appl Physiol* 2013;114:707–715.
- Svenningsen S, Kirby M, Starr D, et al. Hyperpolarized ^3He and ^{129}Xe MRI: Differences in asthma before bronchodilation. *J Magn Reson Imaging* 2013;38:1521–1530.
- Deppe MH, Parra-Robles J, Ajraoui S, et al. Susceptibility effects in hyperpolarized ^3He lung MRI at 1.5T and 3T. *J Magn Reson Imaging* 2009;30:418–423.
- Parra-Robles J, Ajraoui S, Marshall H, Deppe MH, Xu X, Wild JM. The influence of field strength on the apparent diffusion coefficient of ^3He gas in human lungs. *Magn Reson Med* 2012;67:322–325.
- Mathew L, Evans A, Ouriadov A, et al. Hyperpolarized ^3He magnetic resonance imaging of chronic obstructive pulmonary disease. Reproducibility at 3.0 Tesla. *Acad Radiol* 2008;15:1298–1311.
- Parraga G, Ouriadov A, Evans A, et al. Hyperpolarized ^3He ventilation defects and apparent diffusion coefficients in chronic obstructive pulmonary disease: Preliminary results at 3.0 Tesla. *Invest Radiol* 2007;42:384–391.
- Woodhouse N, Wild JM, Van Beek EJR, Hoggard N, Barker N, Taylor CJ. Assessment of hyperpolarized ^3He lung MRI for regional evaluation of interventional therapy: A pilot study in pediatric cystic fibrosis. *J Magn Reson Imaging* 2009;30:981–988.
- O'Sullivan B, Couch M, Roche JP, et al. Assessment of repeatability of hyperpolarized gas MR ventilation functional imaging in cystic fibrosis. *Acad Radiol* 2014;21:1524–1529.
- Ebner L, He M, Virgincar RS, et al. Hyperpolarized ^{129}Xe magnetic resonance imaging to quantify regional ventilation differences in mild to moderate asthma. *Invest Radiol* 2017;52:120–127.
- Shukla Y, Wheatley A, Kirby M, et al. Hyperpolarized ^{129}Xe magnetic resonance imaging. Tolerability in healthy volunteers and subjects with pulmonary disease. *Acad Radiol* 2012;19:941–951.
- Morbach AE, Gast KK, Schmiedeskamp J, et al. Diffusion-weighted MRI of the lung with hyperpolarized helium-3: A study of reproducibility. *J Magn Reson Imaging* 2005;21:765–774.
- Diaz S, Casselbrant I, Piitulainen E, et al. Hyperpolarized ^3He apparent diffusion coefficient MRI of the lung: Reproducibility and volume

- dependency in healthy volunteers and patients with emphysema. *J Magn Reson Imaging* 2008;27:763–770.
27. Norquay G, Collier GJ, Rao M, et al. Large-scale production of highly-polarized ^{129}Xe . In: *Proc 25th Annual Meeting ISMRM, Honolulu*; 2017. p 2140.
 28. Horn FC, Tahir BA, Stewart NJ, et al. Lung ventilation volumetry with same-breath acquisition of hyperpolarized gas and proton MRI. *NMR Biomed* 2014;27:1461–1467.
 29. Wild JM, Ajraoui S, Deppe MH, et al. Synchronous acquisition of hyperpolarised ^3He and ^1H MR images of the lungs — maximising mutual anatomical and functional information. *NMR Biomed* 2011;24:130–134.
 30. Tzeng Y-S, Lutchen K, Albert M. The difference in ventilation heterogeneity between asthmatic and healthy subjects quantified using hyperpolarized ^3He MRI. *J Appl Physiol* 2009;106:813–822.
 31. Marshall H, Deppe MH, Parra-Robles J, et al. Direct visualisation of collateral ventilation in COPD with hyperpolarised gas MRI. *Thorax* 2012;67:613–617.
 32. Pellegrino R, Viegi G, Brusasco V, et al. Interpretative strategies for lung function tests. *Eur Respir J* 2005;26:948–968.
 33. Ajraoui S, Lee KJ, Deppe MH, Parnell SR, Parra-Robles J, Wild JM. Compressed sensing in hyperpolarized ^3He lung MRI. *Magn Reson Med* 2010;63:1059–1069.
 34. Deppe MH, Parra-Robles J, Marshall H, Lanz T, Wild JM. A flexible 32-channel receive array combined with a homogeneous transmit coil for human lung imaging with hyperpolarized ^3He at 1.5 T. *Magn Reson Med* 2011;66:1788–1797.
 35. Chan HF, Stewart NJ, Parra-Robles J, Collier GJ, Wild JM. Whole lung morphometry with 3D multiple b-value hyperpolarized gas MRI and compressed sensing. *Magn Reson Med* 2017;77:1916–1925.
 36. Chan H-F, Stewart NJ, Norquay G, Collier GJ, Wild JM. 3D diffusion-weighted ^{129}Xe MRI for whole lung morphometry. *Magn Reson Med* 2017; DOI: 10.1002/mrm.26960 [Epub ahead of print].
 37. Fичеле S, Paley MNJ, Woodhouse N, Griffiths PD, Van Beek EJR, Wild JM. Investigating ^3He diffusion NMR in the lungs using finite difference simulations and in vivo PGSE experiments. *J Magn Reson* 2004;167:1–11.
 38. Hathaway EH, Tashkin DP, Simmons MS. Intraindividual variability in serial measurements of D l CO and alveolar volume over one year in eight healthy subjects using three independent measuring systems. *Am Rev Respir Dis* 1989;140:1818–1822.